THE JOURNAL OF
PHYSICAL CHEMISTRY
LETTERS
A JOURNAL OF THE AMERICAN CHEMICAL SOCIETY

pubs.acs.org/JPCL

Perspective

Møller–Plesset Adiabatic Connection Theory for Diverse Noncovalent Interactions

Etienne Palos,*,† Heng Zhao,† Kimberly J. Daas, Eduardo Fabiano, Francesco Paesani, and Stefan Vuckovic*

Cite This: https://doi.org/10.1021/acs.jpclett.5c01304

Read Online

ACCESS | Metrics & More | Article Recommendations | Supporting Information

ABSTRACT: Møller–Plesset adiabatic connection (MPAC) theory provides a powerful framework for constructing approximations to wave function-based correlation energy, enabling modeling of noncovalent interactions (NCIs) with near-CCSD(T) accuracy. We show that approximate MPAC functionals consistently outperform MP2 and dispersion-corrected DFT (DFT+DISP) across diverse systems, including charged and charge-transfer complexes. MPAC functionals operate holistically at the electronic level, require no heuristic dispersion corrections, and achieve near-chemical accuracy even for abnormal NCIs, cases where DFT+DISP errors exceed those of DFT. To further improve MPAC for abnormal cases without compromising overall performance, we introduce MPAC25, a simple two-parameter functional treating neutral and charged NCIs equally, as demonstrated on DES15K benchmarks. Overall, MPAC functionals effectively describe a wide range of NCIs, including those beyond the reach of other methods, representing a significant step toward predictive simulations of molecular interactions in complex environments and motivating further MPAC developments.

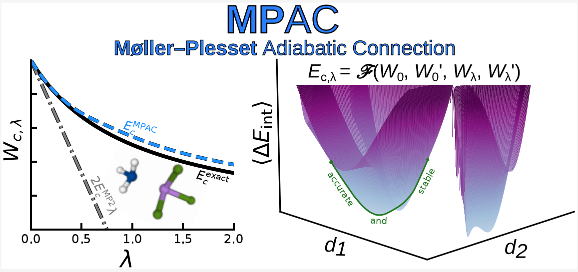

The fundamental role that noncovalent interactions (NCIs) play in phenomena across chemical, condensed matter, and biology[1−7] has motivated the development of electronic structure theory to improve their description, traditionally within correlated wave function theory (WFT)[8] and density functional theory (DFT)[9,10] and, more recently, machine-learning approaches.[11] Accurate modeling of NCIs requires, at the very least, capturing long-range correlation effects such as van der Waals dispersion,[12,13] while for more complex systems, capturing the coupling between dispersion and other effects (e.g., electrostatics, polarization) becomes also important. As such, correlated wave function theory (WFT) methods provide naturally accurate descriptions of NCIs, offering physical insights and benchmarks for approximate methods. Currently, coupled cluster (CC) theory with single, double, and perturbative triple excitations, i.e., CCSD(T),[14,15] serves as the "gold standard" *ab initio* method for NCI energies in single-reference systems, when extrapolated to the complete basis set (CBS) limit.[16] However, the steep $O(N^7)$ scaling of CCSD(T) restricts its application to modest-sized systems, whereas many-body perturbation theory (MBPT) and modern DFT methods provide practical alternatives, although each comes with its own strengths and limitations. Recent developments in reduced-scaling CCSD(T) approximations (e.g., LNO-CCSD(T)[17,18] and DLPNO-CCSD(T)[19,20]) and modern quantum Monte Carlo (MC) techniques (e.g., FN-DMC[21,22] and AF-QMC)[23,24] enabled modeling of systems of size beyond the reach of canonical CCSD(T), yet with comparable accuracy. This, in turn, has led to a better understanding of the accuracy of modern DFT methods (e.g., range-separated hybrid and double hybrid functionals) and MBPT, particularly Møller–Plesset perturbation theory (MPn),[25−27] for predicting NCI energies. Second-order Møller–Plesset perturbation theory [MP2; $O(N^5)$][28] captures some of the long-range correlation effects that semilocal DFT misses and has thus been widely used to study NCIs in molecular clusters. However, while MP2 often performs well for electrostatics-dominated systems,[29] it often overestimates dispersion[30−33] and underestimates polarizability,[34] both crucial for accurately modeling a broad class of NCIs, including ion−π[35] and parallel-displaced π−π interactions.[36−38] Furthermore, it has been shown that the MPn perturbation series may diverge for large complexes, significantly limiting the applicability of MP2 for such systems.[38] Several notable modifications and further developments of MBPT for simulating NCIs have been thoroughly reviewed,[27,39] ranging from semiempirical improvements such as spin-component scaling (e.g., SCS-MP2, SOS-MP2)[40,41] and regularization (κ-MP2),[42−44] to formal NCI frameworks such as SAPT[45] and

Received: April 29, 2025
Revised: July 10, 2025
Accepted: July 10, 2025

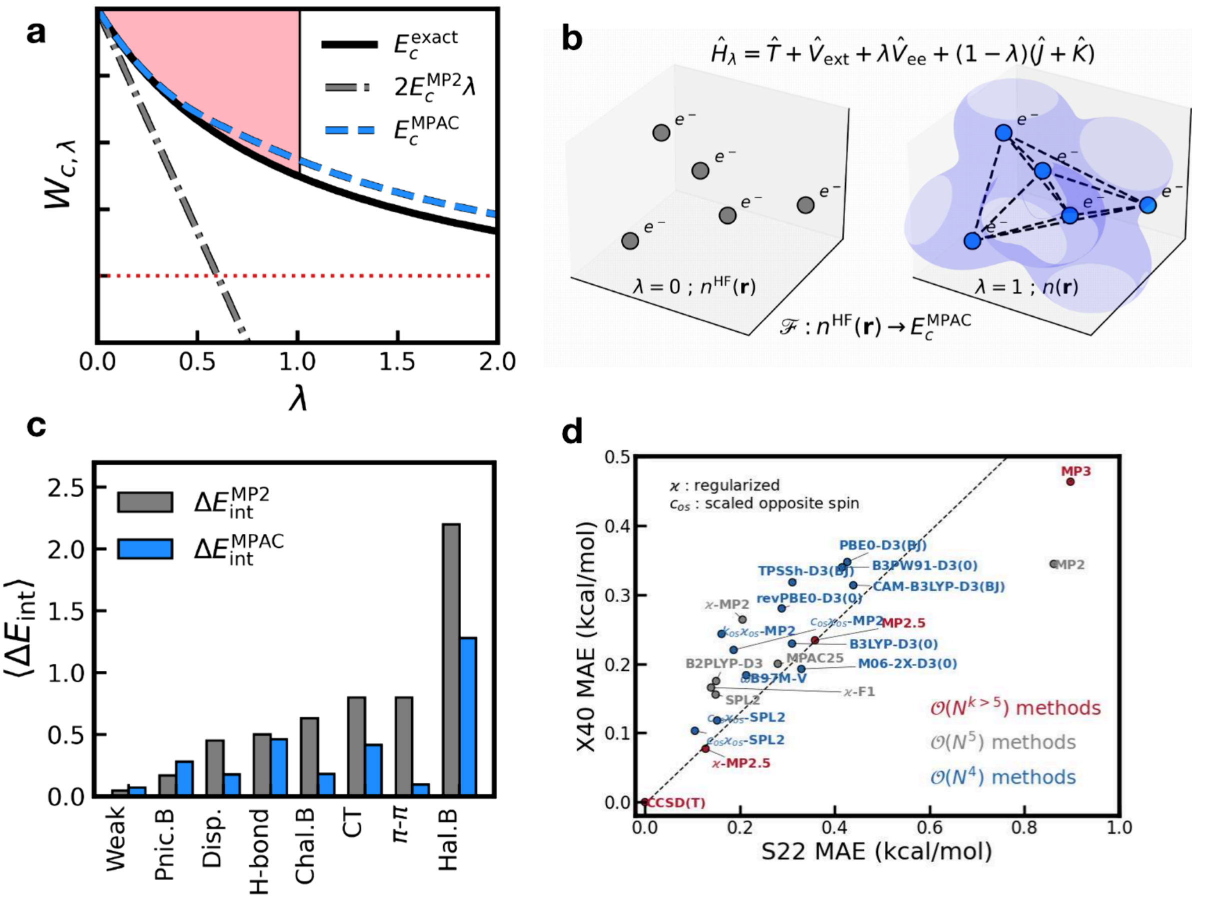

Figure 1. Overview of the MPAC framework: (a) The AC curve for correlation energy E_c is shown: exact MPAC (black), MPAC functional (blue dashed), and MP2 (gray dash-dot). (b) Schematic of the MPAC Hamiltonian $\hat{H}_\lambda$, mapping the noninteracting HF system ($\lambda = 0$) to the fully interacting system ($\lambda = 1$), connecting $n^{\mathrm{HF}}(\mathbf{r})$ to E_c^{MPAC}. (c) Average errors of MPAC and MP2 across various NCIs data sets. (d) MPAC performance against MPn, DFT methods, and CCSD(T), with color-coded computational scaling: N^4 (teal), N^5 (blue), N^{5+} (magenta), with data adapted from ref 74.

related approaches.[46] While *ab initio* methods for NCIs have significantly advanced, the most widely used approach today remains dispersion-corrected DFT (DFT+DISP).[47−50] Several DISP correction models have been developed, including the popular DFT-Dx series (D2,[51] D3,[52] D4,[53] and their variants[54−57]), the many-body dispersion (MBD) family,,[58−64] the exchange-dipole model (XDM).[65] In contrast to empirical DISP corrections, an alternative approach to modeling dispersion is offered by nonlocal van der Waals functionals,[66] such as VV10[67] and its revised form rVV10.[68] Nonlocal correlation functionals play a critical role in capturing dispersion in modern density functionals, including the range-separated hybrid ωB97M-V.[69]

The widespread success of DFT+DISP effectively addresses what was once recognized as a key challenge in DFT.[48,70] For many systems, this improved performance of DFT+DISP over DFT is expected and is what we refer to here as *normal systems*. However, there remain challenging NCI-bound systems for which DFT+DISP either does not improve upon or even *worsens* the base DFT results; we refer to these as *abnormal systems*. For many abnormal systems, particularly charged complexes, results worsen compared to base DFT regardless of what specific DISP correction is added (e.g., D3 or XDM).[71] In this context, a large-scale analysis of several DFT+DISP methods across the DES15K[72] with diverse NCIs,[73] confirms that charged molecular systems remain a challenge for DFT+DISP and for the field in general. Furthermore, abnormal DFT+DISP behavior has been reported for charge-transfer complexes,[74] aqueous ions, such as those in the WATER27[75] data set, and even pure water.[76−78] Identifying abnormal NCIs is also important for molecular simulation practices. For example, ref 79 found revPBE more accurate than revPBE-D3 for alkali ion−water interactions. These challenges underscore the need for robust, yet affordable, methods that do not require heuristic DISP corrections and can treat normal and abnormal NCIs on equal footing.

In this spirit, the recently developed Møller−Plesset adiabatic connection (MPAC)[80,81] framework and resulting approximate functionals emerges as a promising approach for accurate modeling of NCIs.[29,74,81,82] The scaling of MPAC functionals is governed by their E_c^{MP2} component, but unlike double hybrids DFT,[83] MPAC functionals approximate correlation energy within a WFT framework. This prompts the question: If MPAC functionals use E_c^{MP2}, do they naturally inherit the MP2 deficiencies for NCIs? They *do not*, as MPAC functionals use forms that mimic the features of the exact MPAC integrand that yields correlation energy within this framework, in which E_c^{MP2} is used for what it truly represents; one-half of the initial slope of the underlying integrand. The MPAC functionals accurately capture dispersion at the foundational electronic level as they operate at the level of the MPAC integrand, and thus the need for any subsequent

https://doi.org/10.1021/acs.jpclett.5c01304
J. Phys. Chem. Lett. XXXX, XXX, XXX−XXX

dispersion corrections is eliminated (i.e., everything happens holistically at the electronic level). Despite depending nonlinearly on the ingredients, MPAC functionals are size consistent for fragments with nondegenerate ground states,[84] outperform MP2 and state-of-the-art DFT+DISP methods for established NCI data sets, including $\pi-\pi$ complexes such as those in L7[85] and charge-transfer complexes such as those in CT7.[86]

This perspective has two main objectives. First, we review the successes of MPAC for NCIs through the lens of our working definition of normal and abnormal NCIs. We then show that, in addition to achieving high accuracy for normal NCIs, MPAC functionals outperform both MP2 and DFT +DISP in abnormal cases. Second, we show that a more careful parametrization of the first-generation MPAC functional can further improve accuracy for abnormal NCIs without sacrificing performance on normal cases. Finally, our new test results show that the reparameterized MPAC functional achieves high accuracy on a representative DES15k subset, including both neutral and the more challenging charged complexes.

Møller–Plesset Adiabatic Connection Theory. Consider a Hartree–Fock (HF) system that can be connected through a continuous path to the physical system, through the following Hamiltonian:

$$\hat H_\lambda = \hat T + \lambda \hat V_{\mathrm{ee}} + \hat V_{\mathrm{ext}} + (1-\lambda)(\hat J + \hat K) \tag{1}$$

where λ is the coupling constant, $\hat T$, $\hat V_{\mathrm{ext}}$, $\lambda \hat V_{\mathrm{ee}}$, are the kinetic energy, the external potential, and the electron repulsion operators respectively, and $\hat J$ and $\hat K$ represent the Coulomb and exchange operators that depend on the HF orbitals. The noninteracting Hartree–Fock system ($\lambda = 0$) and the physical system ($\lambda = 1$) are connected via the MPAC integrand $W_{\mathrm{c},\lambda} = \langle \Psi_\lambda | \hat V_{\mathrm{ee}} - (\hat J + \hat K) | \Psi_\lambda \rangle - \langle \Psi_0 | \hat V_{\mathrm{ee}} - (\hat J + \hat K) | \Psi_0 \rangle$, which is distinct from the density-fixed DFT AC integrand.[87] The exact WFT-based correlation energy E_{c}, defined as the difference between the exact and HF energy, is obtained from the MPAC integrand, $E_{\mathrm{c}} = \int_0^1 W_{\mathrm{c},\lambda}\, \mathrm{d}\lambda$. Importantly, the MPAC framework provides a powerful route for developing DFT-like approximations that directly map HF densities $n^{\mathrm{HF}}(\mathbf{r})$ to the corresponding WFT-based correlation energy.[80,88] As a result, MPAC functionals inherently use HF densities rather than self-consistent ones due to the fundamental nature of the theory itself, and not merely as a practical heuristic (e.g., as in density-corrected DFT[76,89−92]) to improve results. An important feature of the MPAC is that, in contrast to DFT AC, the electronic density is not fixed in the former, such that the MPAC recovers the HF density $n^{\mathrm{HF}}(\mathbf{r})$ at $\lambda = 0$ and the physical density $n(\mathbf{r})$ at $\lambda = 1$, and the small-λ expansion $W^{\mathrm{HF}}_{c,\lambda\to 0}$ recovers Møller–Plesset perturbation theory, i.e. the MP*n* series.[80,93,94] A core concept of MPAC theory lies in the curvature of the exact $W_{c,\lambda}$, which is crucial for capturing dispersion as it has been revealed that dispersion typically increases the curvature in the MPAC curve.[29] This is illustrated schematically in Figure 1a, where it is also shown that MP*n* approximates $W_{c,\lambda}$ by a straight line, given by $2\lambda E_{\mathrm{c}}^{\mathrm{MP2}}$. The *linear* behavior of MP2 along the AC curve directly enables assessing its reliability for NCIs via curvature strength from an MPAC functional.[29]

As the MPAC functionals are designed by the interpolation between the small and large λ limits of the MPAC, we also note that in this large λ limit (distinct from the large-λ limit of DFT[95−106]), is governed by the functionals of $n^{\mathrm{HF}}(\mathbf{r})$, with the $W_{\mathrm{c},\lambda\to\infty}$ being a leading order term. Gradient expansion approximations,[81] size-consistency corrections (see below),[84] global interpolation schemes, and most recently the correlation energy densities have been investigated for the MPAC,[88] as well as nonempirical strategies for constructing MPAC functionals.[107]

As said and now illustrated in Figure 1b, a key strength of the exact MPAC features (e.g., its large-λ limit being a functional of n^{HF}) is that they provide a rigorous framework for mapping $n^{\mathrm{HF}}(\mathbf{r})$ to E_{c}, irrespective of the accuracy of n^{HF} itself. Note that the WFT-based correlation energy obtained from an approximate MPAC functional will be denoted by $E_{\mathrm{c}}^{\mathrm{MPAC}}$, to distinguish it clearly from the exact E_{c}.

Interaction Energies from MPAC Functionals. Consider a molecular system composed of N interacting fragments, with energy E given by the sum of the Hartree–Fock energy E_{HF} and $E_{\mathrm{c}}^{\mathrm{MPAC}}$.

$$E(N) = E_{\mathrm{HF}}(N) + E_{\mathrm{c}}^{\mathrm{MPAC}}(N) \tag{2}$$

Within the MPAC framework, $E_{\mathrm{c}}^{\mathrm{MPAC}}(N)$ is approximated by a function $\mathcal{F}(\mathbf{W}(N))$ that nonlinearly depends on nonempirical quantities $\mathbf{W}(N)$, which are informed by the $\lambda \to 0$ and $\lambda \to \infty$ limits of the underlying MPAC. The crucial NCI quantity is interaction energy E_{int} defined as the difference between the energy of the N fragment system and the sum of n individual fragments in their actual geometries. For the MPAC functionals, correlation interaction energy is evaluated as

$$\begin{aligned} \Delta E_{\mathrm{c,int}}^{\mathrm{MPAC}} &= E_{\mathrm{c}}^{\mathrm{MPAC}}(N) - \sum_{n=1}^{N} E_{\mathrm{c}}^{\mathrm{MPAC}}(n_i) \\ &= \mathcal{F}(\mathbf{W}(N)) - \mathcal{F}\Big(\sum_{n=1}^{N} \mathbf{W}(n_i)\Big) \end{aligned} \tag{3}$$

to guarantee size-consistency despite the nonlinear dependence of $E_{\mathrm{c}}^{\mathrm{MPAC}}$ on the input ingredients.[82,84] To define approximate functionals for $E_{\mathrm{c}}^{\mathrm{MPAC}}$ in terms of $\mathbf{W}$ explicitly, we can write

$$E_{\mathrm{c}}^{\mathrm{MPAC}} := \mathcal{F}(W_0, W_0', W_\infty, W_\infty') \tag{4}$$

where $W_0 = E_{\mathrm{x}}^{\mathrm{HF}}$ is the HF exchange energy and $W_0' = 2E_{\mathrm{c}}^{\mathrm{MP2}}$; note that it is possible to use only the opposite-spin component, $E_{\mathrm{c}}^{\mathrm{MP2(os)}}$ for reduced $\mathcal{O}(N^4)$ scaling.[74] Both W_0 and W_0' govern the small-λ limit, while W_∞,W_∞' depend on $n^{\mathrm{HF}}(\mathbf{r})^{4/3}$ and $|\nabla n^{\mathrm{HF}}(\mathbf{r})|^2/n^{\mathrm{HF}}(\mathbf{r})^{4/3}$ and $n^{\mathrm{HF}}(\mathbf{r})^{3/2}$ and $|\nabla n^{\mathrm{HF}}(\mathbf{r})|^2/n^{\mathrm{HF}}(\mathbf{r})^{7/6}$, respectively, and describe the $\lambda \to \infty$ limit typically approximated by the point-charge continuum (PC) approximation, as detailed in ref 82.

Different MPAC approximations to $E_{\mathrm{c}}^{\mathrm{MPAC}}$ vary in the level of information from eq 4 they incorporate and in their degree of empiricism. For example, the Seidl–Perdew–Levy (SPL)[95] successor, SPL2, introduced in ref 82 has shown very good results for NCI energies, especially for large NCI complexes (e.g., L7[85] data set). Additionally, a direct approximation to $E_{\mathrm{c}}^{\mathrm{HF}}$ was introduced, known as the "Møller–Plesset Adiabatic Connection Functional 1" form or MPACF1, which will be discussed in detail later. The MPACF1 form represents a first-generation approximation explicitly designed from exact MPAC features, rather than being adapted from existing DFT-AC forms (e.g., SPL2). It provides a foundation for further developing minimally empirical MPAC functionals

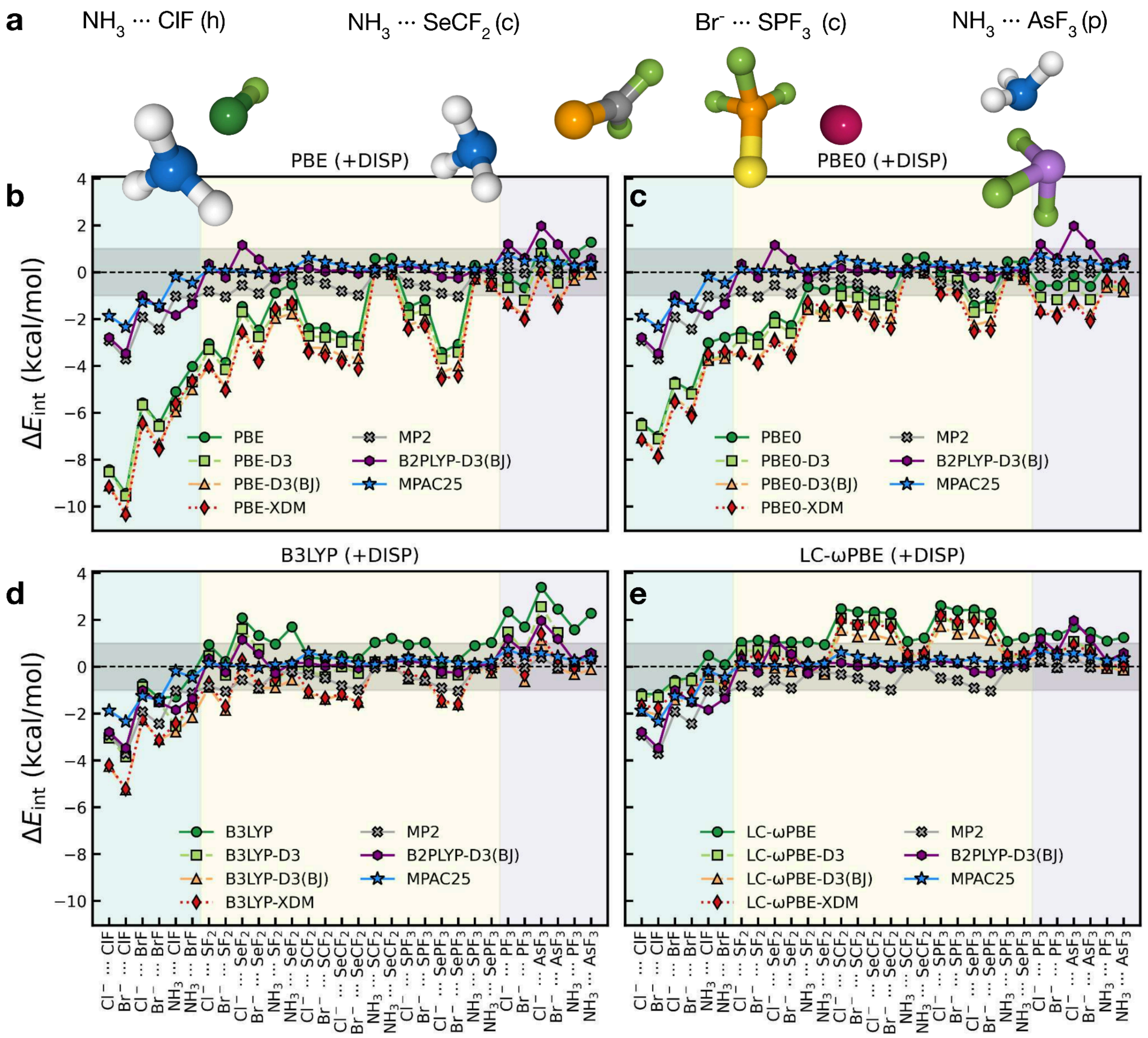

Figure 2. Proof of concept for abnormal NCIs using B30 as a case study: (a) Representative halogen (h), chalcogen (c), and pnictogen (p) bonded complexes. (b−e) Interaction energy errors (kcal/mol) for various functionals with/without dispersion: PBE, PBE0, B3LYP, and LC-*ω*PBE. Across all cases, adding dispersion worsens performance relative to the bare functional. MPAC25 (blue), MP2 (gray) and the double-hyrbid functional B2PLYP-D3(BJ) (purple) are shown for comparison.

such as MPAC25 (see below) and more advanced forms like the recently introduced HFAC24.[107] Additionally, regularization and spin-opposite component scaling led to the κ-F1 and $c_{os}\kappa_{os}$-SPL-2, which are MPAC functionals that outperform MP2 in both accuracy and efficiency.[74] The relative accuracy of MPAC functionals compared to MP2 for different NCIs is shown in Figure 1, and a comparison between MPAC functionals to existing methods in terms scaling with *N* is shown in Figure 1d.

Horizontally shaded regions denote bonding types. DFT +DISP and CCSD(T) data was obtained from ref 108.

Identifying and Addressing Normal and Abnormal NCIs. To compare MPAC and DFT+DISP performance for NCIs, we recall our working definitions: an NCI complex is *normal* if adding DISP corrections improves accuracy relative to uncorrected DFT, and *abnormal* otherwise. As we shall see, this distinction highlights the advantage of MPAC over DFT +DISP, as the former provides a holistic framework capable of accurately describing both classes of NCIs. Examples of abnormal systems reported in the literature include charge-transfer complexes, charge−π, and charge−dipole interactions.[74,108,109] To illustrate the difference between normal and abnormal cases when comparing MPAC and DFT+DISP, we use the B30 data set,[110] which contains examples of both. The B30 set includes halogen, chalcogen, and pnictogen bonded complexes, and Figure 2b−e shows errors for several DFT +DISP methods in decreasing order of the B30 delocalization error.[111] From Figure 2, it is clear that including exact exchange, either through global (PBE0, B3LYP) or range-separated (LC-*ω*PBE) hybrids, improves B30 accuracy over GGAs (PBE). However, *reducing* delocalization error alone is insufficient to eliminate the abnormal behavior, as seen for PBE0+DISP and B3LYP+DISP. Figure 2 also shows that MPAC25 (built below) consistently outperforms hybrid DFT +DISP mehtods, the double-hybrid B2PLYP+D3(BJ) method, and MP2 across the entire B30 set. Remarkably, MPAC25 is the only method predicting B30 interaction energies within ∼1% (on average) of the CCSD(T) references.

To better understand the benefit MPAC functionals offer over DFT+DISP for abnormal cases, we explore the relation-

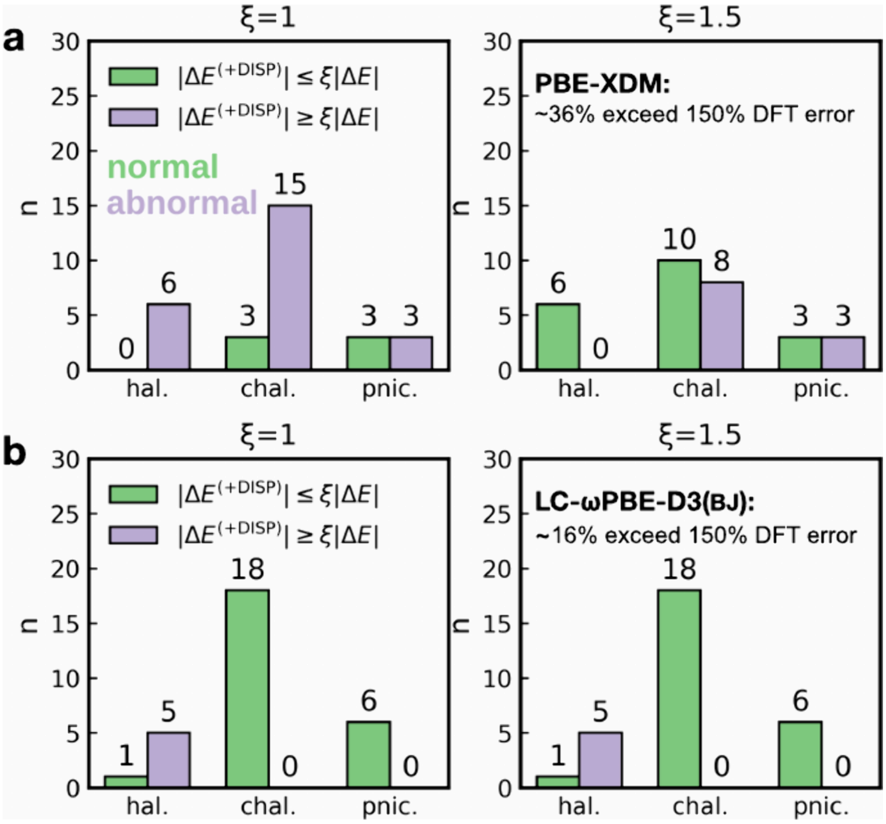

Figure 3. Bar plot of reaction counts in B30 data set satisfying $|\Delta E_{\mathrm{int}}^{\mathrm{DFT+DISP}}| \le \xi|\Delta E_{\mathrm{int}}^{\mathrm{DFT}}|$ for two DFT+DISP methods and different ξ values: (a) PBE+XDM, the worst performer for B30, and (b) LC-ωPBE-D3(BJ), the best performer considered in this work. The number of normal cases is associated with the green bars, while the abnormal cases are shown in purple.

ship between DFT+DISP methods and normal—abnormal behavior using the inequality linking the two errors, $|\Delta E_{\mathrm{int}}^{\mathrm{DFT+DISP}}| \le \xi|\Delta E_{\mathrm{int}}^{\mathrm{DFT}}|$, where $\xi < \xi_c$ indicates normal cases for an appropriate value ξ_c. With this inequality and without attempting to set a strict boundary, we roughly classify B30 cases as normal and abnormal, focusing on the trends robust to variations in ξ, the base DFT, and the DISP correction. For example, Figure 3a counts the number of normal and abnormal B30 complexes based on the inequality above, at $\xi = 1$ and $\xi = 1.5$ and with PBE-XDM. We can see that PBE-XDM performs worse than PBE alone for 24 out of 30 complexes (left); in 11 of which, the error of PBE-XDM is over 1.5 times larger than the PBE error (right).

On the other hand, Figure 3b shows that LC-ωPBE+D3(BJ) yields only 5 abnormal cases (all halogen-bonded). However, for these 5 cases, even for LC-ωPBE+D3(BJ), the best-performing DFT+DISP method here with lower delocalization error than PBE, the error still exceeds 150% of the base LC-ωPBE error. This analysis highlights how, from semilocal to range-separated hybrid functionals, charged halogen-bonded complexes remain abnormal. While MPAC25 predicts ~86% of B30 within chemical accuracy, we note that 4 halogen-bonded systems fall outside of this threshold, confirming that these abnormal cases are the most challenging NCIs in the set, independently of the method.

Still, the overall high accuracy of MPAC25 for B30 is evident from its mean absolute error (MAE) being below 0.5 kcal/mol, as shown in Figure 4 for several methods, plotted from the lowest MAE to the highest MAE. The 3 most accurate methods are MPAC functionals (MPAC25, SPL2, and MPACF1) and provide comparable accuracy in a range of ~0.2 kcal/mol. The MPAC functionals are followed by the

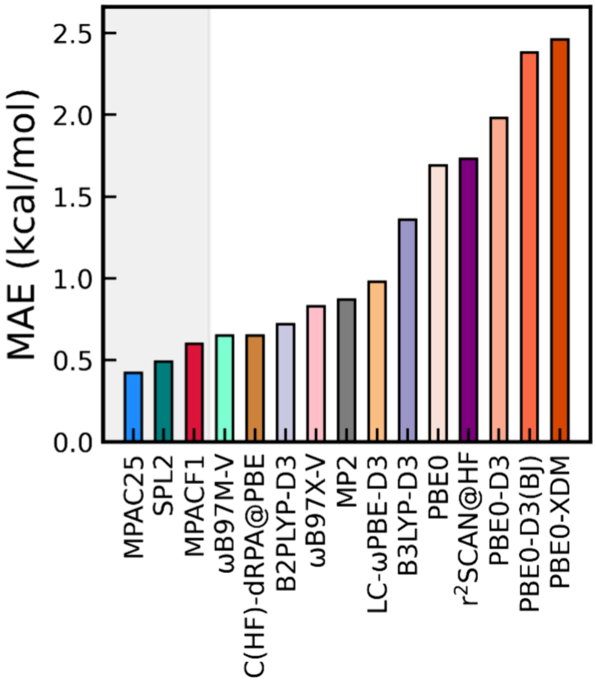

Figure 4. Performance on the B30 data set: mean absolute error (MAE) in kcal/mol for several electronic structure methods, ranked from lowest (MPAC25) to highest (PBE0-XDM).

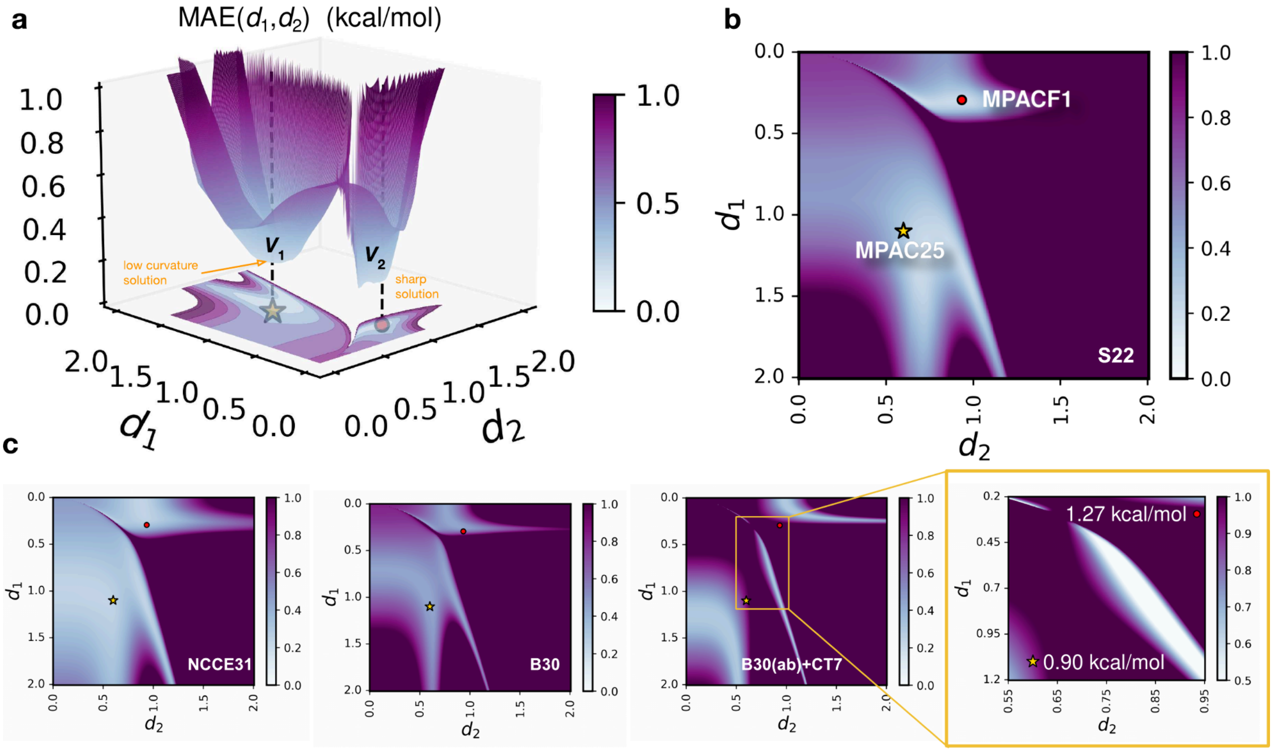

Figure 5. (a) Surface representation of [d_1, d_2] parameter space for the MPACF1 functional with the MAE (kcal/mol) associated with the S22 data set along the z axis and (b) detailed heatmap of [$d_1 d_2$] dependence. Our proposed parameters are represented by the orange star in well V_1, while the red dot represents the parameters from ref 82 in well V_2. (c) Heatmaps of [d_1, d_2] parameter space for different test data sets: NCCE31, S66×8, B30, and "abnormal" complexes in B30, as identified in the previous analysis.

range-separated meta-GGA ωB97M-V,[69] and double hybrids such as B2PLYP-D3(BJ).[112]

MPAC25 Model. So far, we have shown the results for MPAC25, which we obtain in this perspective from the MPACF1 correlation energy form

$$E_{c,\lambda}^{\alpha,\beta} := -g^{\alpha,\beta}\lambda + g^{\alpha,\beta}\left(\frac{[h^{\alpha,\beta}(d_1, d_2) + 1]\lambda}{\sqrt{d_1^2\lambda + 1} + [h^{\alpha,\beta}(d_1, d_2)]^4\sqrt{d_2^2\lambda + 1}}\right) \tag{5}$$

where the functionals $g^{\alpha,\beta} = -W_{c,\infty}^{\alpha,\beta}$ and $h^{\alpha,\beta}(d_1, d_2) = (-E_c^{\mathrm{MP2}} - 2d_1^2 W_{c,\infty}^{\alpha,\beta})(-E_c^{\mathrm{MP2}} + 2d_2^4 W_{c,\infty}^{\alpha,\beta})^{-1}$ as in ref 82. In addition, $W_{c,\infty}^{\alpha,\beta}$ is approximated as $W_{c,\infty}^{\alpha,\beta} = \alpha W_{c,\infty}^{\mathrm{DFT}} + \beta E_x^{\mathrm{HF}}[\{\phi_i^{\mathrm{HF}}\}]$, following the relation in the large-λ limit $W_{c,\infty}^{\alpha,\beta} \leq W_{c,\infty}^{\mathrm{DFT}}$, as demonstrated in ref 81. Here, we obtain MPAC25 by reparameterizing the original MPACF1 functional,[82] resulting in an even more balanced description of normal and abnormal NCIs, as detailed below.

Next, we discuss the relationship between MPACF1 and MPAC25 in terms of generalizability across diverse NCIs. eq 5 involves parameters α, β, d_1, d_2, which can be fitted (see ref 74). However, imposing the physical constraint $\alpha = \beta = 1$, which ensures recovery of the uniform electron gas as $\lambda \to \infty$, leaves only d_1 and d_2 to be fitted. Another advantage of the MPACF1 form in eq 5 is that it exhibits the correct large-λ asymptotic behavior, unlike the more empirical SPL2 functional and its variants. By analyzing the parameter robustness of MPACF1, we show that the MPAC25 parameters ($\alpha = \beta = 1$, $d_1 = 1.1$, $d_2 = 0.6$) improve over the original parametrization.

Figure 5a shows the MAE landscape as a function of d_1 and d_2 for the S22 data set, originally used to fit MPACF1 and other MPAC functionals. We identify two regions of interest in this landscape: V_1, associated with MPAC25 (orange star), and V_2, associated with the original MPACF1 (red circle).

MPACF1 parameters (d_1 = 0.294, d_2 = 0.934) were originally chosen by minimizing the MAE on S22.[82] Here, we investigate whether parameters located in region V_1 provide improved generalizability across diverse NCIs without significantly sacrificing accuracy on the original S22 training set. Notably, the minimum in V_2 (red circle) achieves a slightly lower MAE for S22 compared to the MPAC25 (orange star in V_1). However, the curvature around the MPAC25 parameters (orange star, V_1) in the MAE landscape (Figure 5a and b) is significantly flatter than around the original MPACF1 parameters (red circle, V_2). Indeed, refitting parameters with minimal curvature constraints gives an MAE of 0.20 kcal/mol on S22, only 0.01 kcal/mol above the original MPACF1MAE (0.19 kcal/mol).[82] Further details are provided in the Supporting Information. Importantly, the flatter landscape around the orange star indicates improved generalizability[113] beyond the S22 training set. This is confirmed by Figure 5c, which shows the MAE landscape for the NCCE31 and B30 data sets, both containing normal and abnormal NCIs. For NCCE31, the MAE landscape is similar to that of S22 (Figure 5b), with MPAC25 and MPACF1 achieving MAEs of 0.25 and 0.33 kcal/mol, respectively. For B30, the MAE landscape notably changes, placing MPACF1 (red circle) at the edge of the sharper V_2 region. Finally, we isolate the abnormal cases in the last panel of Figure 5c, combining B30(ab) and CT7 sets (CT7 is Charge Transfer 7 in NCCE31). Interestingly, this is where the MAE landscape and accuracy of the two models (MPAC25 in V_1 and MPACF1 in V_2) differs most substantially. Namely, for these abnormal cases, only MPAC25 achieves chemical accuracy with an MAE of 0.90

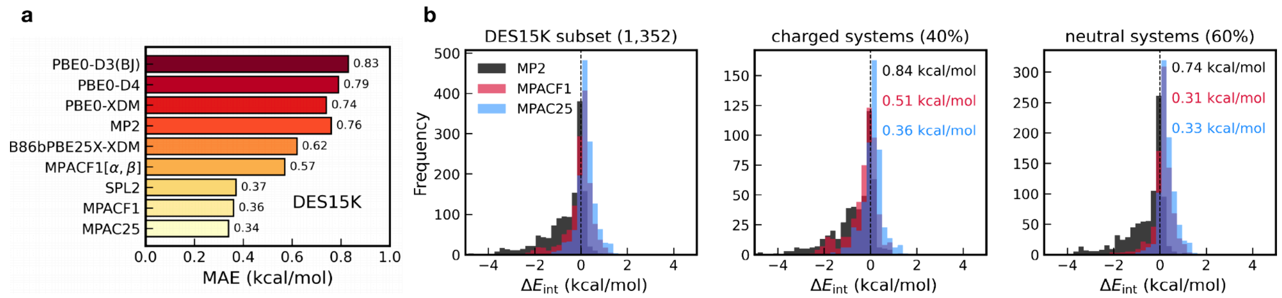

Figure 6. Analysis of a subset from the D.E. Shaw 15K (DES15K) database[72] with MPAC25 and other methods. (a) MAE (kcal/mol) is shown for 9 methods from MPAC25 (light yellow) to PBE0-D3(BJ) (blood red), showing that MPAC25 is the best performer across DES15K structures, and highlights that MPAC models offer similar performance (MAE ≤ 0.6 kcal/mol), surpassing MP2 and a variety of dispersion corrected hybrid functionals and MP2. The MAES for all DFT methods were obtained from ref 73. (b) Histogram of errors is shown for MPAC25 (blue) and MPACF1 (red) for 1352 complexes, of which 853 are neutral and 499 are charged.

kcal/mol, improving over MPACF1 by 0.37 kcal/mol (1.27 kcal/mol).

These analyses demonstrate that minimally empirical MPAC functionals can be improved by leveraging parameter regions with flatter error landscapes, such as V_1. Such flatter regions indicate greater robustness and generalizability beyond the original S22 training set, thus providing improved accuracy for abnormal NCIs without sacrificing performance on normal cases.

Performance of MPAC for DES15K Subset. After reviewing MPAC performance for NCIs and introducing MPAC25 to improve treatment of abnormal cases, we now evaluate MPAC functionals against an additional benchmark. Specifically, we construct a representative subset from the DES15K data set, to include diverse interaction types. Our DES15K subset includes 1352 molecular dimers, where 853 (∼60%) are neutral and 499 (∼40%) are charged nonmetal complexes. MP2 and MPAC energies have been computed by extrapolation to the complete basis set limit (see Computational Details). The MAES of the DFT+DISP methods for our DES15K subset are comparable to those reported for the full DES15K data set,[73] despite the fact that the former comprises only a small fraction (∼10%) of the latter.

Figure 6a shows the MAEs (kcal/mol) for several methods, ordered from lowest (MPAC25) to highest (PBE0-XDM). Notably, MPAC-based methods (MPAC25, MPACF1, SPL2, and MPACF1[α, β]) achieve the four lowest MAEs across the 1352 complexes, with MPAC25 as the best performing method (MAE ∼ 0.30 kcal/mol). All MPAC functionals considered here achieve MAEs below 0.60 kcal/mol, outperforming the best DFT+DISP method tested (hybrid B86bPBE25X-XDM, MAE = 0.62 kcal/mol). Finally, MPAC25 achieves less than half the MAE of MP2 for the DES15K subset, consistent with previous benchmarks showing large improvements of MPAC over MP2 for NCIs.[74] In addition to the MAEs (Figure 6a), Table 1 shows RMSEs for all methods, separately for neutral (825) and charged (527) subsets (additional statistics are in the Supporting Information), confirming that MPAC25 consistently outperforms MPACF1, especially for charged complexes (by ∼0.25 kcal/mol), without sacrificing accuracy for neutral systems.

Overall, these results establish MPAC25 as a promising and robust "workhorse" functional for quantum-chemical simulations of NCIs, demonstrating improved accuracy over the 4-parameter SPL2 on our DES15K subset, while also having a stronger physical foundation derived from the exact MPAC features. Finally, following ref 74, MPAC25 can be made more efficient by spin-opposite component scaling[114] (c_{os}-MPAC25), as illustrated in the Supporting Information.

Table 1. Root Mean Square Error (RMSE) in kcal/mol for Different Methods in Full, Charged, and Neutral Sets[a]

method	full	charged	neutral
PBE0-D3(BJ)	1.30	2.04	0.80
PBE0-D4	1.26	1.96	0.79
PBE0-XDM	1.18	1.80	0.77
MP2	1.27	1.34	1.22
B86bPBE25X-XDM	1.01	1.57	0.62
MPACF1[α, β]	0.79	0.75	0.82
SPL2	0.51	0.48	0.53
MPACF1	0.56	0.69	**0.47**
MPAC25	**0.45**	**0.44**	**0.47**

[a] The lowest value in each column is in bold. Errors reported with respect to CCSD(T)/CBS reference energies.[72].

Summary and Outlook. In summary, in this perspective, we reviewed and extended functionals based on the Møller–Plesset adiabatic connection theory focusing on their performance for modeling NCIs. MPAC functionals approximate wave function-based correlation energy by interpolating between the small- and large-λ limits of MPAC. As such, the inherent advantage of MPAC functionals for modeling NCIs is that they operate entirely at the electronic level, requiring no heuristic corrections to capture dispersion. Second, unlike double hybrids, MPAC functionals do not rely on error cancellations between exact exchange, MP2 correlation, and their semilocal counterparts. Instead, they incorporate exact exchange and MP2 correlation in full as input quantities defining their small-λ limit. As a result of these advantages, MPAC functionals consistently provide near-CCSD(T) accuracy for diverse NCIs, with major improvements over MP2 and state-of-the-art dispersion-corrected DFT (DFT+DISP), particularly for abnormal NCIs where DFT+DISP exhibits large inaccuracies.

We have also introduced MPAC25, a minimally empirical functional that accurately models charged and neutral, as well as normal and abnormal NCIs within a unified framework, which can be further improved by combining specific machine-learning techniques[115,116] and MPAC correlation energy densities.[88]

Practical MPAC applications have thus far focused on relatively small systems, highlighting the importance of extending MPAC to larger N-body systems, motivated by recent studies revealing limitations of DFT- and MP2-based approaches for such systems.[77,78,109,117−120] For example, the performance of MPAC for complex *solute–solvent* systems relevant to chemistry and biochemistry[121] is yet to be explored. Furthermore, extending MPAC to N-body systems will enable data-driven many-body[122] and MPAC-based machine-learning potentials,[123] facilitating accurate condensed-phase simulations on the nanosecond time scale. This would represent a crucial advance in *ab initio* simulations, though implementing MPAC forces remains an essential step to realize this goal.

Computational Details. The data associated with the MPAC ingredients **W** for the S22, NCCE31 and B30 data sets were obtained from ref 74. The DFT(+DISP) data for the B30 analysis was obtained from refs 108, 124, and 125. The DFT(+DISP) data for the DES15K analysis was obtained from ref 73. In relation to DES15K, all MP2 calculations employed the resolution of identity approximation as implemented in TURBOMOLE,[126] and were approximated in the complete basis set limit. The complete basis set limit was estimated using 2-point extrapolation with the aug-cc-pVDZ and aug-cc-pVTZ basis sets (D/T). Finally, the Boys–Bernardi counterpoise correction was applied to account for basis set superposition error. Further computational details can be found in the Supporting Information.

ASSOCIATED CONTENT

Data Availability Statement

The data that support the findings of this study are available within the main manuscript and its Supporting Information. Additional raw data and the Python code for analyses can also be found on Zenodo in ref (XX) and ref (XX), respectively.

Supporting Information

The Supporting Information is available free of charge at https://pubs.acs.org/doi/10.1021/acs.jpclett.5c01304.

Interaction energy values in kcal/mol associated with the B30 analysis for all functionals included in Figure 2, abnormal NCI count as a function of ξ for different functionals supporting Figure 3, MAE values associated with Figure 4, $[d_1, d_2]$ surfaces of NCCE31, B30, and B30(ab)+CT7 associated with the heat maps in Figure 5, loss landscape and heatmap of S66×8, details on $[d_1, d_2]$ optimization, table with MAE, MSE, RMSE, and MAX error associated with Figure 6 and Table 1, and table with all MPAC ingredients for B30, NCCE31, and S22 (PDF)

AUTHOR INFORMATION

Corresponding Authors

Etienne Palos – *Department of Chemistry and Biochemistry, University of California, San Diego, La Jolla, California 92093, United States;* orcid.org/0000-0003-2171-0792; Email: epalos@ucsd.edu

Stefan Vuckovic – *Department of Chemistry, Faculty of Science and Medicine, Université de Fribourg/Universitäat Freiburg, CH-1700 Fribourg, Switzerland;* orcid.org/0000-0002-0768-9176; Email: stefan.vuckovic@unifr.ch

Authors

Heng Zhao – *Department of Chemistry, Faculty of Science and Medicine, Université de Fribourg/Universitäat Freiburg, CH-1700 Fribourg, Switzerland;* orcid.org/0009-0001-6162-9203

Kimberly J. Daas – *Department of Chemistry, University of California, Irvine, Irvine, California 92697, United States;* orcid.org/0000-0002-4323-6908

Eduardo Fabiano – *Institute for Microelectronics and Microsystems (CNR-IMM), 73100 Lecce, Italy; Center for Biomolecular Nanotechnologies, Istituto Italiano di Tecnologia, 73010 Arnesano, Italy;* orcid.org/0000-0002-3990-669X

Francesco Paesani – *Department of Chemistry and Biochemistry, Materials Science and Engineering, and San Diego Supercomputer Center, University of California, San Diego, La Jolla, California 92093, United States;* orcid.org/0000-0002-4451-1203

Complete contact information is available at: https://pubs.acs.org/10.1021/acs.jpclett.5c01304

Author Contributions

†Etienne Palos and Heng Zhao contributed equally to this work.

Notes

The authors declare no competing financial interest.

ACKNOWLEDGMENTS

E.P. acknowledges support from National Science Foundation (NSF) Graduate Research Fellowship Program (GRFP) through Grant DGE-2038238, the Alfred P. Sloan Ph.D. Fellowship through Grant G-2020-14067, the State Secretariat for Education, Research and Innovation (SERI) for supporting his stay in Switzerland through the ThinkSwiss Research Scholarship program, and allocation CHE240150 from the Advanced Cyberinfrastructure Coordination Ecosystem: Services & Support (ACCESS) program, which is supported by NSF GRFP Grant DGE-2038238. K.J.D. acknowledges support from the UCI Chancellor's Postdoctoral Fellowship Program and in particular Prof. Dr. Feizal Waffarn for his support as a sponsor. E.F. acknowledges support from MUR-PRIN 2022 through Grant 2022LM2K5X, CUP: B53D23004320006 funded by European Union - NextGenerationEU-PNRR. F.P. acknowledges support from the National Science Foundation through Grant 2311260. S.V. acknowledges support from the Swiss National Science Foundation (SNSF) Starting Grant Project TMSGI2 211246.

REFERENCES

(1) Stone, A. *The Theory of Intermolecular Forces*; Oxford University Press: Oxford, U.K., 2013.

(2) Anslyn, E. V.; Dougherty, D. A. *Modern Physical Organic Chemistry*; University Science Books: Sausalito, CA, 2004.

(3) Schalley, C. A. *Analytical Methods in Supramolecular Chemistry*, 2nd ed.; Wiley: Hoboken, NJ, 2012.

(4) Cockroft, S. L.; Hunter, C. A. Chemical Double-Mutant Cycles: Dissecting Non-Covalent Interactions. *Chem. Soc. Rev.* **2007**, *36*, 172–188.

(5) Brown, T. L.; Bursten, B. E.; Eugene, H.; LeMay, H. *Chemistry: The Central Science*, 11th ed.; Pearson Prentice Hall: Upper Saddle River, NJ, 2009.

(6) Eisler, M. In *Encyclopedia of Nanoscience and Society*; Guston, D. H., Ed.; SAGE Publications: Thousand Oaks, CA, 2010.

(7) Biedermann, F.; Schneider, H.-J. Experimental Binding Energies in Supramolecular Complexes. *Chem. Rev.* **2016**, *116*, 5216–5300.

(8) Helgaker, T.; Jorgensen, P.; Olsen, J. *Molecular Electronic-Structure Theory*; John Wiley & Sons: Hoboken, NJ, 2013.

(9) Hohenberg, P.; Kohn, W. Inhomogeneous Electron Gas. *Phys. Rev.* **1964**, *136*, B864.

(10) Kohn, W.; Sham, L. J. Self-Consistent Equations Including Exchange and Correlation Effects. *Phys. Rev.* **1965**, *140*, A1133.

(11) Kirkpatrick, J.; McMorrow, B.; Turban, D. H. P.; Gaunt, A. L.; Spencer, J. S.; Matthews, A. G. D. G.; Obika, A.; Thiry, L.; Fortunato, M.; Pfau, D.; Castellanos, L. R.; Petersen, S.; Nelson, A. W. R.; Kohli, P.; Mori-Sánchez, P.; Hassabis, D.; Cohen, A. J. Pushing the Frontiers of Density Functionals by Solving the Fractional Electron Problem. *Science* **2021**, *374*, 1385−1389.

(12) London, F. Zur theorie und systematik der molekularkräfte. *Zeitschrift für Physik* **1930**, *63*, 245−279.

(13) London, F. The general theory of molecular forces. *Trans. Faraday Soc.* **1937**, *33*, 8b−26.

(14) Raghavachari, K.; Trucks, G. W.; Pople, J. A.; Head-Gordon, M. A fifth-order perturbation comparison of electron correlation theories. *Chem. Phys. Lett.* **1989**, *157*, 479−483.

(15) Stanton, J. F. Why CCSD(T) Works: a Different Perspective. *Chem. Phys. Lett.* **1997**, *281*, 130−134.

(16) Rezac, J.; Hobza, P. Benchmark Calculations of Interaction Energies in Noncovalent Complexes and Their Applications. *Chem. Rev.* **2016**, *116*, 5038−5071.

(17) Nagy, P. R.; Kállay, M. Approaching the basis set limit of CCSD(T) energies for large molecules with local natural orbital coupled-cluster methods. *J. Chem. Theory Comput.* **2019**, *15*, 5275−5298.

(18) Nagy, P. R. State-of-the-art local correlation methods enable affordable gold standard quantum chemistry for up to hundreds of atoms. *Chem. Sci.* **2024**, *15*, 14556−14584.

(19) Guo, Y.; Riplinger, C.; Becker, U.; Liakos, D. G.; Minenkov, Y.; Cavallo, L.; Neese, F. Communication: An Improved Linear Scaling Perturbative Triples Correction for the Domain Based Local Pair-Natural Orbital Based Singles and Doubles Coupled Cluster Method [DLPNO-CCSD(T)]. *J. Chem. Phys.* **2018**, *148*, 011101.

(20) Jiang, A.; Schaefer III, H. F.; Turney, J. M. Linear-Scaling Local Natural Orbital-Based Full Triples Treatment in Coupled-Cluster Theory. *J. Chem. Theory Comput.* **2025**, *21*, 2386−2401.

(21) Foulkes, W. M.; Mitas, L.; Needs, R.; Rajagopal, G. Quantum Monte Carlo simulations of solids. *Rev. Mod. Phys.* **2001**, *73*, 33.

(22) Dubecky, M.; Mitas, L.; Jurecka, P. Noncovalent interactions by quantum Monte Carlo. *Chem. Rev.* **2016**, *116*, 5188−5215.

(23) Zhang, S.; Krakauer, H. Quantum Monte Carlo method using phase-free random walks with Slater determinants. *Physical review letters* **2003**, *90*, 136401.

(24) Lee, J.; Pham, H. Q.; Reichman, D. R. Twenty years of auxiliary-field quantum Monte Carlo in quantum chemistry: An overview and assessment on main group chemistry and bond-breaking. *J. Chem. Theory Comput.* **2022**, *18*, 7024−7042.

(25) Møller, C.; Plesset, M. S. Note on an approximation treatment for many-electron systems. *Physical review* **1934**, *46*, 618.

(26) Pople, J. A.; Binkley, J. S.; Seeger, R. Theoretical models incorporating electron correlation. *Int. J. Quantum Chem.* **1976**, *10*, 1−19.

(27) Cremer, D. Møller−Plesset perturbation theory: from small molecule methods to methods for thousands of atoms. *WIREs Comput. Mol. Sci.* **2011**, *1*, 509−530.

(28) Binkley, J.; Pople, J. Møller−Plesset theory for atomic ground state energies. *Int. J. Quantum Chem.* **1975**, *9*, 229−236.

(29) Vuckovic, S.; Fabiano, E.; Gori-Giorgi, P.; Burke, K. MAP: an MP2 accuracy predictor for weak interactions from adiabatic connection theory. *J. Chem. Theory Comput.* **2020**, *16*, 4141−4149.

(30) Tsuzuki, S.; Honda, K.; Uchimaru, T.; Mikami, M.; Tanabe, K. Origin of Attraction and Directionality of the π/π Interaction: Model Chemistry Calculations of Benzene Dimer Interaction. *J. Am. Chem. Soc.* **2002**, *124*, 104−112.

(31) Grimme, S. Do Special Noncovalent $\pi-\pi$ Stacking Interactions Really Exist? *Angew. Chem., Int. Ed. Engl.* **2008**, *47*, 3430−3434.

(32) Tkatchenko, A.; DiStasio, R. A.; Head-Gordon, M.; Scheffler, M. Dispersion-Corrected Møller-Plesset Second-Order Perturbation Theory. *J. Chem. Phys.* **2009**, *131*, 094106.

(33) Hohenstein, E. G.; Sherrill, C. D. Wavefunction Methods for Noncovalent Interactions. *WIREs Comput. Mol. Sci.* **2012**, *2*, 304−326.

(34) Nguyen, B. D.; Hernandez, D. J.; Flores, E. V.; Furche, F. Dispersion size-consistency. *Electronic Structure* **2022**, *4*, 014003.

(35) Lao, K. U.; Schäffer, R.; Jansen, G.; Herbert, J. M. Accurate description of intermolecular interactions involving ions using symmetry-adapted perturbation theory. *J. Chem. Theory Comput.* **2015**, *11*, 2473−2486.

(36) Schramm, B.; Gray, M.; Herbert, J. M. Substituent and Heteroatom Effects on $\pi-\pi$ Interactions: Evidence That Parallel-Displaced π-Stacking is Not Driven by Quadrupolar Electrostatics. *J. Am. Chem. Soc.* **2025**, *147*, 3243−3260.

(37) Riley, K. E.; Platts, J. A.; Rezac, J.; Hobza, P.; Hill, J. G. Assessment of the Performance of MP2 and MP2 Variants for the Treatment of Noncovalent Interactions. *J. Phys. Chem. A* **2012**, *116*, 4159−4169.

(38) Nguyen, B. D.; Chen, G. P.; Agee, M. M.; Burow, A. M.; Tang, M. P.; Furche, F. Divergence of many-body perturbation theory for noncovalent interactions of large molecules. *J. Chem. Theory Comput.* **2020**, *16*, 2258−2273.

(39) Beran, G. J.; Greenwell, C.; Cook, C.; Rezac, J. Improved Description of Intra-and Intermolecular Interactions through Dispersion-Corrected Second-Order Møller−Plesset Perturbation Theory. *Acc. Chem. Res.* **2023**, *56*, 3525−3534.

(40) Grimme, S. Improved second-order Møller−Plesset perturbation theory by separate scaling of parallel-and antiparallel-spin pair correlation energies. *J. Chem. Phys.* **2003**, *118*, 9095−9102.

(41) Grimme, S.; Goerigk, L.; Fink, R. F. Spin-component-scaled electron correlation methods. *WIREs Comput. Mol. Sci.* **2012**, *2*, 886−906.

(42) Stück, D.; Head-Gordon, M. Regularized orbital-optimized second-order perturbation theory. *J. Chem. Phys.* **2013**, *139*, 244109.

(43) Lee, J.; Head-Gordon, M. Regularized orbital-optimized second-order Møller−Plesset perturbation theory: A reliable fifth-order-scaling electron correlation model with orbital energy dependent regularizers. *J. Chem. Theory Comput.* **2018**, *14*, 5203−5219.

(44) Shee, J.; Loipersberger, M.; Rettig, A.; Lee, J.; Head-Gordon, M. Regularized second-order Møller−Plesset theory: A more accurate alternative to conventional MP2 for noncovalent interactions and transition metal thermochemistry for the same computational cost. *J. Phys.: Condens. Matter* **2021**, *12*, 12084−12097.

(45) Szalewicz, K. Symmetry-adapted perturbation theory of intermolecular forces. *WIREs Comput. Mol. Sci.* **2012**, *2*, 254−272.

(46) Williams, H. L.; Chabalowski, C. F. Using Kohn- Sham Orbitals in Symmetry-Adapted Perturbation Theory to Investigate Intermolecular Interactions. *J. Phys. Chem. A* **2001**, *105*, 646−659.

(47) Grimme, S. Density Functional Theory With London Dispersion Corrections. *WIREs Comput. Mol. Sci.* **2011**, *1*, 211−228.

(48) Kristyán, S.; Pulay, P. Can (semi) local density functional theory account for the London dispersion forces? *Chem. Phys. Lett.* **1994**, *229*, 175−180.

(49) Gianturco, F.; Paesani, F. *Conceptual Perspectives in Quantum Chemistry*; Springer: Dordrecht, Netherlands, 1997; pp 337−382.

(50) Gianturco, F.; Paesani, F.; Laranjeira, M.; Vassilenko, V.; Cunha, M. Intermolecular forces from density functional theory. III. A multiproperty analysis for the Ar (1 S)-CO (1 Σ) interaction. *J. Chem. Phys.* **1999**, *110*, 7832−7845.

(51) Grimme, S. Semiempirical GGA-type density functional constructed with a long-range dispersion correction. *Journal of computational chemistry* **2006**, *27*, 1787−1799.

(52) Grimme, S.; Antony, J.; Ehrlich, S.; Krieg, H. A consistent and accurate *ab initio* parametrization of density functional dispersion correction (DFT-D) for the 94 elements H-Pu. *J. Chem. Phys.* **2010**, *132*, 154104.

(53) Caldeweyher, E.; Bannwarth, C.; Grimme, S. Extension of the D3 dispersion coefficient model. *J. Chem. Phys.* **2017**, *147*, 034112.

(54) Grimme, S.; Ehrlich, S.; Goerigk, L. Effect of the damping function in dispersion corrected density functional theory. *J. Comput. Chem.* **2011**, *32*, 1456−1465.

(55) Witte, J.; Mardirossian, N.; Neaton, J. B.; Head-Gordon, M. Assessing DFT-D3 damping functions across widely used density functionals: Can we do better? *J. Chem. Theory Comput.* **2017**, *13*, 2043−2052.

(56) Tkachenko, N. V.; Dittmer, L. B.; Tomann, R.; Head-Gordon, M. Smooth dispersion is physically appropriate: Assessing and amending the D4 dispersion model. *J. Phys.: Condens. Matter* **2024**, *15*, 10629−10637.

(57) Tkachenko, N. V.; Head-Gordon, M. Smoother Semiclassical Dispersion for Density Functional Theory via D3S: Understanding and Addressing Unphysical Minima in the D3 Dispersion Correction Model. *J. Chem. Theory Comput.* **2024**, *20*, 9741−9753.

(58) Axilrod, B.; Teller, E. Interaction of the van der Waals type between three atoms. *J. Chem. Phys.* **1943**, *11*, 299−300.

(59) Muto, Y. Force between nonpolar molecules. *J. Phys. Math. Soc. Jpn.* **1943**, *17*, 629−631.

(60) Anatole von Lilienfeld, O.; Tkatchenko, A. Two-and Three-Body Interatomic Dispersion Energy Contributions to Binding in Molecules and Solids. *J. Chem. Phys.* **2010**, *132*, 234109.

(61) Tkatchenko, A.; DiStasio, R. A., Jr.; Car, R.; Scheffler, M. Accurate and Efficient Method for Many-Body Van der Waals Interactions. *Phys. Rev. Lett.* **2012**, *108*, 236402.

(62) Gould, T.; Lebegue, S.; Angyan, J. G.; Bučko, T. A fractionally ionic approach to polarizability and van der Waals many-body dispersion calculations. *J. Chem. Theory Comput.* **2016**, *12*, 5920−5930.

(63) Kim, M.; Kim, W. J.; Gould, T.; Lee, E. K.; Lebègue, S.; Kim, H. uMBD: A materials-ready dispersion correction that uniformly treats metallic, ionic, and van der Waals bonding. *J. Am. Chem. Soc.* **2020**, *142*, 2346−2354.

(64) Xu, P.; Alkan, M.; Gordon, M. S. Many-Body Dispersion. *Chem. Rev.* **2020**, *120*, 12343−12356.

(65) Becke, A. D.; Johnson, E. R. Exchange-Hole Dipole Moment and the Dispersion Interaction: High-Order Dispersion Coefficients. *J. Chem. Phys.* **2006**, *124*, 014104.

(66) Dion, M.; Rydberg, H.; Schröder, E.; Langreth, D. C.; Lundqvist, B. I. Van der Waals density functional for general geometries. *Physical review letters* **2004**, *92*, 246401.

(67) Vydrov, O. A.; Van Voorhis, T. Nonlocal van der Waals density functional: The simpler the better. *J. Chem. Phys.* **2010**, *133*, 244103.

(68) Sabatini, R.; Gorni, T.; de Gironcoli, S. Nonlocal van der Waals density functional made simple and efficient. *Physical Review B: Condensed Matter and Materials Physics* **2013**, *87*, 041108.

(69) Mardirossian, N.; Head-Gordon, M. ωB97M-V: A Combinatorially Optimized Range-Separated Hybrid Meta-GGA Density Functional With VV10 Nonlocal Correlation. *J. Chem. Phys.* **2016**, *144*, 214110.

(70) Cohen, A. J.; Mori-Sánchez, P.; Yang, W. Challenges for Density Functional Theory. *Chem. Rev.* **2012**, *112*, 289−320.

(71) Dasgupta, S.; Palos, E.; Pan, Y.; Paesani, F. Balance between physical interpretability and energetic predictability in widely used dispersion-corrected density functionals. *J. Chem. Theory Comput.* **2024**, *20*, 49−67.

(72) Donchev, A. G.; Taube, A. G.; Decolvenaere, E.; Hargus, C.; McGibbon, R. T.; Law, K.-H.; Gregersen, B. A.; Li, J.-L.; Palmo, K.; Siva, K.; Bergdorf, M.; Klepeis, J. L.; Shaw, D. E. Quantum chemical benchmark databases of gold-standard dimer interaction energies. *Scientific Data* **2021**, *8*, 55.

(73) Nickerson, C. J.; Bryenton, K. R.; Price, A. J.; Johnson, E. R. Comparison of density-functional theory dispersion corrections for the DES15K database. *J. Phys. Chem. A* **2023**, *127*, 8712−8722.

(74) Daas, K. J.; Kooi, D. P.; Peters, N. C.; Fabiano, E.; Della Sala, F.; Gori-Giorgi, P.; Vuckovic, S. Regularized and Opposite Spin-Scaled Functionals from Møller−Plesset Adiabatic Connection — Higher Accuracy at Lower Cost. *J. Phys.: Condens. Matter* **2023**, *14*, 8448−8459.

(75) Manna, D.; Kesharwani, M. K.; Sylvetsky, N.; Martin, J. M. Conventional and explicitly correlated ab initio benchmark study on water clusters: Revision of the BEGDB and WATER27 data sets. *J. Chem. Theory Comput.* **2017**, *13*, 3136−3152.

(76) Vuckovic, S.; Song, S.; Kozlowski, J.; Sim, E.; Burke, K. Density Functional Analysis: the Theory of Density-Corrected DFT. *J. Chem. Theory Comput.* **2019**, *15*, 6636−6646.

(77) Sharkas, K.; Wagle, K.; Santra, B.; Akter, S.; Zope, R. R.; Baruah, T.; Jackson, K. A.; Perdew, J. P.; Peralta, J. E. Self-Interaction Error Overbinds Water Clusters but Cancels in Structural Energy Differences. *Proc. Natl. Acad. Sci. U.S.A.* **2020**, *117*, 11283−11288.

(78) Dasgupta, S.; Lambros, E.; Perdew, J. P.; Paesani, F. Elevating density functional theory to chemical accuracy for water simulations through a density-corrected many-body formalism. *Nat. Commun.* **2021**, *12*, 6359.

(79) Kostal, V.; Mason, P. E.; Martinez-Seara, H.; Jungwirth, P. Common cations are not polarizable: Effects of dispersion correction on hydration structures from ab initio molecular dynamics. *J. Phys.: Condens. Matter* **2023**, *14*, 4403−4408.

(80) Seidl, M.; Giarrusso, S.; Vuckovic, S.; Fabiano, E.; Gori-Giorgi, P. Communication: Strong-interaction limit of an adiabatic connection in Hartree-Fock theory. *J. Chem. Phys.* **2018**, *149*, 241101.

(81) Daas, K. J.; Grossi, J.; Vuckovic, S.; Musslimani, Z. H.; Kooi, D. P.; Seidl, M.; Giesbertz, K. J. H.; Gori-Giorgi, P. Large coupling-strength expansion of the Møller−Plesset adiabatic connection: From paradigmatic cases to variational expressions for the leading terms. *J. Chem. Phys.* **2020**, *153*, 214112.

(82) Daas, K. J.; Fabiano, E.; Della Sala, F.; Gori-Giorgi, P.; Vuckovic, S. Noncovalent interactions from models for the Møller−Plesset adiabatic connection. *J. Phys.: Condens. Matter* **2021**, *12*, 4867−4875.

(83) Zhang, Y.; Xu, X.; Goddard, W. A., III Doubly hybrid density functional for accurate descriptions of nonbond interactions, thermochemistry, and thermochemical kinetics. *Proc. Natl. Acad. Sci. U.S.A.* **2009**, *106*, 4963−4968.

(84) Vuckovic, S.; Gori-Giorgi, P.; Della Sala, F.; Fabiano, E. Restoring size consistency of approximate functionals constructed from the adiabatic connection. *J. Phys.: Condens. Matter* **2018**, *9*, 3137−3142.

(85) Sedlak, R.; Janowski, T.; Pitonak, M.; Rezac, J.; Pulay, P.; Hobza, P. Accuracy of quantum chemical methods for large noncovalent complexes. *J. Chem. Theory Comput.* **2013**, *9*, 3364−3374.

(86) Zhao, Y.; Truhlar, D. G. Benchmark databases for nonbonded interactions and their use to test density functional theory. *J. Chem. Theory Comput.* **2005**, *1*, 415−432.

(87) Polak, E.; Daas, K. J.; Vuckovic, S. *Chemical Modelling*; Royal Society of Chemistry: London, U.K., 2024: Vol. *18*.

(88) Daas, K. J.; Zhao, H.; Polak, E.; Vuckovic, S. Exact Møller−Plesset Adiabatic Connection Correlation Energy Densities. *J. Chem. Theory Comput.* **2025**, *21*, 5501−5513.

(89) Kim, M.-C.; Sim, E.; Burke, K. Understanding and Reducing Errors in Density Functional Calculations. *Phys. Rev. Lett.* **2013**, *111*, 073003.

(90) Kim, M.-C.; Park, H.; Son, S.; Sim, E.; Burke, K. Improved DFT Potential Energy Surfaces via Improved Densities. *J. Phys.: Condens. Matter* **2015**, *6*, 3802−3807.

(91) Sim, E.; Song, S.; Vuckovic, S.; Burke, K. Improving Results by Improving Densities: Density-Corrected Density Functional Theory. *J. Am. Chem. Soc.* **2022**, *144*, 6625−6639.

(92) Song, S.; Vuckovic, S.; Sim, E.; Burke, K. Density-corrected DFT explained: Questions and answers. *J. Chem. Theory Comput.* **2022**, *18*, 817−827.

(93) Pernal, K. Correlation energy from random phase approximations: A reduced density matrices perspective. *Int. J. Quantum Chem.* **2018**, *118*, No. e25462.

(94) Pernal, K. Electron correlation from the adiabatic connection for multireference wave functions. *Phys. Rev. Lett.* **2018**, *120*, 013001.

(95) Seidl, M.; Perdew, J. P.; Levy, M. Strictly correlated electrons in density-functional theory. *Phys. Rev. A* **1999**, *59*, 51.

(96) Seidl, M. Strong-interaction limit of density-functional theory. *Phys. Rev. A* **1999**, *60*, 4387.

(97) Seidl, M.; Perdew, J. P.; Kurth, S. Simulation of all-order density-functional perturbation theory, using the second order and the strong-correlation limit. *Physical review letters* **2000**, *84*, 5070.

(98) Seidl, M.; Perdew, J. P.; Kurth, S. Density functionals for the strong-interaction limit. *Phys. Rev. A* **2000**, *62*, 012502.

(99) Perdew, J. P.; Kurth, S.; Seidl, M. Exploring the adiabatic connection between weak-and strong-interaction limits in density functional theory. *International Journal of Modern Physics B* **2001**, *15*, 1672−1683.

(100) Gori-Giorgi, P.; Seidl, M.; Vignale, G. Density-functional theory for strongly interacting electrons. *Physical review letters* **2009**, *103*, 166402.

(101) Liu, Z.-F.; Burke, K. Adiabatic connection for strictly correlated electrons. *J. Chem. Phys.* **2009**, *131*, 124124.

(102) Gori-Giorgi, P.; Seidl, M. Density functional theory for strongly-interacting electrons: perspectives for physics and chemistry. *Phys. Chem. Chem. Phys.* **2010**, *12*, 14405−14419.

(103) Malet, F.; Gori-Giorgi, P. Strong correlation in Kohn-Sham density functional theory. *Physical review letters* **2012**, *109*, 246402.

(104) Vuckovic, S.; Irons, T. J.; Savin, A.; Teale, A. M.; Gori-Giorgi, P. Exchange−correlation functionals via local interpolation along the adiabatic connection. *J. Chem. Theory Comput.* **2016**, *12*, 2598−2610.

(105) Vuckovic, S.; Irons, T. J.; Wagner, L. O.; Teale, A. M.; Gori-Giorgi, P. Interpolated energy densities, correlation indicators and lower bounds from approximations to the strong coupling limit of DFT. *Phys. Chem. Chem. Phys.* **2017**, *19*, 6169−6183.

(106) Vuckovic, S.; Levy, M.; Gori-Giorgi, P. Augmented potential, energy densities, and virial relations in the weak-and strong-interaction limits of DFT. *J. Chem. Phys.* **2017**, *147*, 214107.

(107) Constantin, L. A.; Fabiano, E.; Della Sala, F. Nonempirical Adiabatic Connection Correlation Functional from Hartree−Fock Orbitals. *J. Phys.: Condens. Matter* **2025**, *16*, 3378−3388.

(108) Kim, Y.; Song, S.; Sim, E.; Burke, K. Halogen and chalcogen binding dominated by density-driven errors. *J. Phys.: Condens. Matter* **2019**, *10*, 295−301.

(109) Palos, E.; Caruso, A.; Paesani, F. Consistent density functional theory-based description of ion hydration through density-corrected many-body representations. *J. Chem. Phys.* **2023**, *159*, 181101.

(110) Bauza, A.; Alkorta, I.; Frontera, A.; Elguero, J. On the reliability of pure and hybrid DFT methods for the evaluation of halogen, chalcogen, and pnicogen bonds involving anionic and neutral electron donors. *J. Chem. Theory Comput.* **2013**, *9*, 5201−5210.

(111) Hait, D.; Head-Gordon, M. Delocalization Errors in Density Functional Theory are Essentially Quadratic in Fractional Occupation Number. *J. Phys.: Condens. Matter* **2018**, *9*, 6280−6288.

(112) Grimme, S. Semiempirical hybrid density functional with perturbative second-order correlation. *J. Chem. Phys.* **2006**, *124*, 034108.

(113) Goodfellow, I.; Bengio, Y.; Courville, A. *Deep Learning*; MIT Press: Cambridge, MA, 2016; Chapter 4, pp 78−93.

(114) Jung, Y.; Lochan, R. C.; Dutoi, A. D.; Head-Gordon, M. Scaled opposite-spin second order Møller−Plesset correlation energy: An economical electronic structure method. *J. Chem. Phys.* **2004**, *121*, 9793−9802.

(115) Polak, E.; Zhao, H.; Vuckovic, S. Real-space machine learning of correlation density functionals. *ChemRxiv* **2024**, DOI: 10.26434/chemrxiv-2024-zk6hp-v2.

(116) Wodynski, A.; Glodny, K.; Kaupp, M. Data-Driven Improvement of Local Hybrid Functionals: Neural-Network-Based Local Mixing Functions and Power-Series Correlation Functionals. *J. Chem. Theory Comput.* **2025**, *21*, 762−775.

(117) Wagle, K.; Santra, B.; Bhattarai, P.; Shahi, C.; Pederson, M. R.; Jackson, K. A.; Perdew, J. P. Self-Interaction Correction in Water−Ion Clusters. *J. Chem. Phys.* **2021**, *154*, 094302.

(118) Palos, E.; Lambros, E.; Swee, S.; Hu, J.; Dasgupta, S.; Paesani, F. Assessing the interplay between functional-driven and density-driven errors in DFT models of water. *J. Chem. Theory Comput.* **2022**, *18*, 3410−3426.

(119) Broderick, D. R.; Herbert, J. M. Delocalization error poisons the density-functional many-body expansion. *Chem. Sci.* **2024**, *15*, 19893−19906.

(120) Broderick, D. R.; Herbert, J. M. Untangling Sources of Error in the Density-Functional Many-Body Expansion. *J. Phys.: Condens. Matter* **2025**, *16*, 2793−2799.

(121) Palos, E.; Zhao, H.; Fontenelle, V.; Paesani, F.; Vuckovic, S. Manuscript in preparation.

(122) Palos, E.; Dasgupta, S.; Lambros, E.; Paesani, F. Data-driven many-body potentials from density functional theory for aqueous phase chemistry. *Chem. Phys. Rev.* **2023**, *4*, 011301.

(123) Bore, S. L.; Paesani, F. Realistic phase diagram of water from "first principles" data-driven quantum simulations. *Nat. Commun.* **2023**, *14*, 3349.

(124) Hernandez, D. J.; Rettig, A.; Head-Gordon, M. A New View on Density Corrected DFT: Can One Get a Better Answer for a Good Reason? *arXiv.org, e-Print Arch., Phys.* **2023**, arXiv:2306.15016.

(125) Graf, D.; Thom, A. J. Corrected density functional theory and the random phase approximation: Improved accuracy at little extra cost. *J. Chem. Phys.* **2023**, *159*, 174106.

(126) Franzke, Y. J.; Holzer, C.; Andersen, J. H.; Begušić, T.; Bruder, F.; Coriani, S.; Della Sala, F.; Fabiano, E.; Fedotov, D. A.; Fürst, S.; et al. TURBOMOLE: Today and tomorrow. *J. Chem. Theory Comput.* **2023**, *19*, 6859−6890.